Influence of realistic EV fleet response with power and energy controllers in an EV-wind virtual power plant

Ledro, Mirko; Calearo, Lisa; Zepter, Jan Martin; Gabderakhmanova, Tatiana; Marinelli, Mattia

Published in:
Sustainable Energy, Grids and Networks

Link to article, DOI:
10.1016/j.segan.2022.100704

Publication date:
2022

Document Version
Publisher's PDF, also known as Version of record

Sustainable Energy, Grids and Networks 31 (2022) 100704

Contents lists available at ScienceDirect

Sustainable Energy, Grids and Networks

journal homepage: www.elsevier.com/locate/segan

Influence of realistic EV fleet response with power and energy controllers in an EV-wind virtual power plant

Mirko Ledro, Lisa Calearo, Jan Martin Zepter, Tatiana Gabderakhmanova, Mattia Marinelli *

Technical University of Denmark, Department of Electrical Engineering, Frederiksborgvej 399, Roskilde, 4000, Denmark

ARTICLE INFO

Article history:
Received 27 July 2021
Received in revised form 8 February 2022
Accepted 13 March 2022
Available online 23 March 2022

Keywords:
Energy management
Power smoothing
Fluctuating RES
EV activation time
EV charging modulation
Virtual power plant

ABSTRACT

To facilitate the integration of volatile renewable energy sources (RES), electric vehicle (EV) fleets are considered valuable flexibility assets. With their storage capability, they can contribute to compensating for fluctuations and providing balancing support when integrated in a virtual power plant (VPP). This paper investigates the response of an EV fleet to wind power fluctuations by accounting for non-synchronized activation time and discrete modulation of the charging current. The influence of the EV fleet response is further investigated comparing a power-based controller with an energy-based one.

Results show that a realistic EV fleet response affects the VPP output more when a power controller is considered. A discrete modulation of the EV charging current can cause oscillations, which would not occur with a linear modulation. Positively, the influence of a non-synchronized EV activation time is negligible for both controllers, proving that a synchronized activation time can be assumed during similar studies. Despite the equality from a mathematical perspective, the hourly VPP energy production when an EV fleet is controlled with a power controller does not correspond to when an energy controller is adopted.

1. Introduction

Environmental concerns are driving the transition towards a higher penetration of renewable energy sources (RESs), such as wind and solar, and flexible electric loads, such as electric vehicles (EVs). On the production side, sudden and barely predictable oscillations of wind speed and solar radiation translate into fluctuating power injections, weakening short-term grid quality and stability [1]. On the consumption side, EVs can potentially stress local grids when considering a large simultaneous charging need. However, they can also offer flexibility, if enabled by smart charging. To align the developments on the production and consumption side, RES generation and EVs consumption can be confined in a virtual power plant (VPP). Coordinated by a fleet aggregator (FA), many EVs are controlled to jointly regulate their charge plan depending on the available RES production. By adjusting their charging power with smart control strategies, larger EV fleets can contribute to compensate for fluctuating RES output.

To this end, different control strategies have been developed in the literature to smooth RES power fluctuations and decreasing the difference between forecasted and actual RES energy production [2]. Two types of controllers are predominant [3]. Power controllers react instantaneously, and rearrange the EV charging set-point continuously depending on the RES power production. Energy controllers, on the contrary, rearrange the EV charging set-point conditional to energy targets, within a certain time window. Depending on the chosen control window, these control actions are less frequent. In the related literature, power and energy controllers have been implemented with different purposes for EV-RES integration. The former has been used to improve grid stability, as in [4] where Vehicle-to-Grid (V2G) charging control is used to stabilize the system frequency and voltage, or in [5] where EVs are controlled to enhance self-consumption of photovoltaic plant (PV), and avoid the injection of intermittent power into the grid. Other investigations focus on the EV perspective, still trying to minimize power fluctuations in the grid but considering the battery lifetime [6], or constraints in terms of SOC and departure time [7]. Differently, the latter controller focuses on market-based analysis and EV charging needs from the energy perspective. Indeed, in [8] EVs are scheduled to match the hourly energy demand with the help of a WF, or in [9] V2G charging is used to supply power reserve to erase mismatches due to forecasting RES errors. From the user needs perspective, in [10] EVs are controlled depending on EV owner behaviour uncertainties to help a WF to participate in several markets, whereas in [11] EVs via V2G maximizes the SOC at plug-out time.

* Corresponding author.
E-mail addresses: mirle@elektro.dtu.dk (M. Ledro), lica@elektro.dtu.dk (L. Calearo), jmwze@elektro.dtu.dk (J.M. Zepter), tatigab@elektro.dtu.dk (T. Gabderakhmanova), matm@elektro.dtu.dk (M. Marinelli).

https://doi.org/10.1016/j.segan.2022.100704

List of Variables and Acronyms

Indices

t	Generic time instant
T	Control window
i	Generic set of EV

Variables

P^{RES}	RES power production
P^{ref}	Reference power signal
P^{EV}	EV fleet charging power
P^{max}	Max P^{EV}
P^{min}	Min P^{EV}
P^{off}	EV fleet offset charging power
P^{ε}	Power error signal
E^{RES}	RES energy production
E^{nom}	RES nominal energy production
$E_T^{\mathrm{RES}^*}$	RES energy target
E^{UB}	Energy value of upper energy band
E^{LB}	Energy value of lower energy band
$E^{\varepsilon\mathrm{UB}}$	Energy error in respect to E^{UB}
$E^{\varepsilon\mathrm{LB}}$	Energy error in respect to E^{LB}
E^{ε}	Energy error signal
I^{set}	EV current set-point
I^{off}	EV offset current set-point
I^{nom}	EV nominal flexibility
I^{max}	Max I^{set}
I^{min}	Min I^{set}
ΔP^{EV}	Deviation in P^{EV}
ΔP^{EV^*}	Admitted deviation in P^{EV}
ΔE^{EV}	Deviation in E^{RES}
$\Delta E_T^{\mathrm{RES}^*}$	Expected deviation in E^{RES}
ΔI^{set}	Deviation in I^{set}
T^{on}	Activation time
T^{FA}	Required time from FA
T^{EV}	EV response delay
T^{B}	Time constant of EV BESS
δt	Minimum time to absorb $\Delta E_T^{\mathrm{RES}^*}$ in T
$\delta\tau$	Maximum waiting time to absorb $\Delta E_T^{\mathrm{RES}^*}$ in T
K_P	Proportional gain
K_I	Integral gain
K_D	Droop gain
N^{EV}	Number of charging EV
V	Voltage level

Acronyms

CH3PH	Unidirectional three-phase charger
CV	Coefficient of variation
EC	Energy controller
EV	Electric vehicle
G1V	Grid-to-Vehicle
FA	Fleet aggregator
MAE	Mean absolute error
PC	Power controller
PI	Proportional–Integral
PV	Photovoltaic plant
RES	Renewable energy source
SOC	State-of-Charge
VPP	Virtual Power Plant
V2G	Vehicle-to-Grid
WF	Wind farm

Despite various analyses with power and energy controllers, a clear comparison between the two, for the suitability of managing an EV fleet, is still missing in the literature. Indeed, authors in [2,3] consider a battery energy storage system (BESS) instead of an EV fleet. Consequently, the influence of the EV fleet response on the performances of these controllers has not been investigated so far in the literature. General assumptions are to consider a linear modulation of the EV charging current, with a synchronized EV charging set-point variation among all EVs in a fleet. These, however, neglect the discrete charging modulation required from real world implementation [12], and the time delay behaviour of charging equipment [13]. Hence, the overall control performance for second-based analysis is distorted. Finally, a constant VPP power production obtained via power controller is mathematically equivalent (from an energy perspective) to guide linearly the VPP energy production via energy controller. Thus, the respective hourly energy produced from the VPP should correspond. However, the authors evidence the lack of proof when the two controllers are applied to an EV fleet.

In this paper, the impact of EV activation time and modulation of EV charging current is analysed when EVs are integrated in VPP with presence of fluctuating RES. The influence of the EV fleet response is investigated when comparing power and energy controllers. Therefore, the contributions of the present manuscript are fourfold:

1. Modelling of pseudo-real EV fleet response with non-synchronized EV activation time and discrete modulation of the charging current.
2. Comparison of power and energy controllers from a modelling perspective, and consequent proof of their non-equivalent energy management.
3. Design of a variable stiffness control logic for the energy controller, and consequent comparison with existing fixed stiffness control logic.
4. Analysis of the EV fleet response influence on the performance of power and energy controllers.

The analysis is based on a EV-wind VPP located at the substation of Aakirkeby on the Danish island of Bornholm. High-resolution 10-s historical wind production data are gathered, and pseudo-real (simulated) Danish driving data for modelling the charging behaviour of the local population are considered. A scenario with 100 % EV penetration in Aakirkeby is reproduced, however it is assumed that only 45 % of all EVs composing the fleet are daily charged. The EVs adjust their charging power as a function of the FA request, and EVs are equipped with unidirectional chargers only (often referred as Grid-to-Vehicle (G1V)). In fact, although the V2G chargers can provide larger flexibility than G1V chargers, they are more complex in terms of infrastructure and therefore subject to high investment costs [14]. Moreover, they require a more sophisticated control logic to assure a minimum SOC at the end of the charging time to satisfy EV owners, which can increase the cycle losses of the battery and accelerate its degradation [15].

The paper is organized as follows. Section 2 describes the methodology for modelling the EV fleet, the power and energy

controllers. Section 3 presents the test case. Section 4 gathers the results and compares the different scenarios. Finally, conclusions and future works are summarized in Section 5.

2. Methodology

The methodology implemented in this article is based on the importance of modelling realistic EV fleet response, and to compare the structure of power and energy controllers for compensating RES fluctuations. For doing this, three elements are needed:

- a fluctuating RES, which provides the power production as one of the input of the EV controllers.
- an EV smart charging controller, whose output is the charging current for the EV fleet.
- an EV fleet, whose charging current is continuously adjusted by the controller to provide support to fluctuating RES.

This section describes the methodology for modelling the last two components: EV fleet and EV smart charging controller. The RES power plant model is out of the scope of this analysis, since historical RES power production data can be directly considered. Section 2.1 describes the EV fleet model to represent both a simplified and a realistic response of the fleet. Two EV smart charging controllers are then presented in Sections 2.2 and 2.3. The first is the power controller and the second is the energy controller. For the sake of readability, all formulas are applied to an entire control window T, here reported for a generic time instant $t \in T$.

2.1. EV fleet model

The EV fleet is modelled with both a simplified and a realistic EV response to the RES output fluctuations. by accounting for EV charging current modulation and EV activation time.

First, each EV is considered grid-connected via a domestic unidirectional charger. Following the IEC 61851 communication standard and based on the selected charger type, the admitted charging range ($I^{\min}$ – $I^{\max}$) is defined [16]. The EV offset current set-point (I^{off}) can be fixed at the average charging value, obtained by (1), so EVs provide a symmetrical regulation in the admitted charging range. Moreover, since real world implementations often require a 1A-discrete modulation, the model allows to adjust the EV current set-point (I^{set}) by linear or 1A-discrete modulation in the charging range (Fig. 1) [12].

$$I^{\text{off}} = \frac{I^{\max} + I^{\min}}{2} \tag{1}$$

Second, between the RES production changes and the EVs response, there is a time delay, defined as mean activation time $\overline{T}^{\text{on}}$.

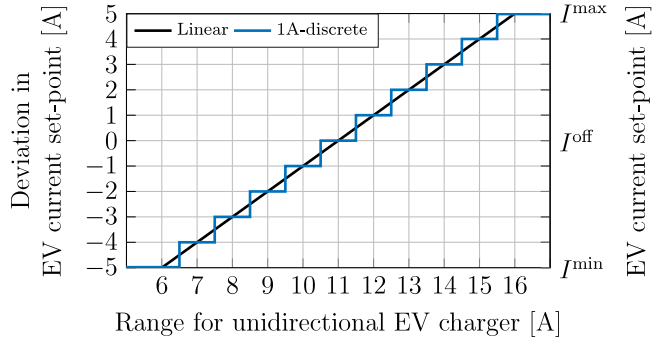

Fig. 1. Modulation of EV current set-point.

Based on measurements from commercial unidirectional chargers [13], $\overline{T}^{\text{on}}$ is considered equal to 3 s and it is the sum of two components

$$\overline{T}^{\text{on}} = T^{\text{FA}} + \overline{T}^{\text{EV}} \tag{2}$$

where:

- T^{FA} is the required time by the FA to gather P^{RES}, compute and send a new I^{set} to the EV fleet, assumed to be equal to 1 s;
- $\overline{T}^{\text{EV}}$ is the mean EV response delay among all EVs in the fleet after receiving a new I^{set}, assumed to be equal to 2 s.

The EV fleet response is represented by the transfer function reported in (3), whose constants and parameters were validated against real EV and charger data in [17]. $\overline{T}^{\text{b}}$ is the mean first-order time constant of the EV batteries and N^{EV} is the number of EVs charging.

$$H(s) = \frac{N^{\text{EV}}}{1 + \overline{T}^{\text{b}} s} e^{-\overline{T}^{\text{EV}} s} \tag{3}$$

Ideally, EVs in the fleet would all respond after $\overline{T}^{\text{EV}}$, and the response would be called synchronized. However, in the reality the vehicles do not respond synchronized, but with stochastic delays related to $\overline{T}^{\text{EV}}$. Thus, additionally to the synchronized EV activation time, a binomial and a uniform discrete probability distribution are here proposed to reproduce the non-synchronized EVs activation time (Fig. 2). For each discrete distribution, the EV fleet is divided into nine sets i of EVs simulating different delays, each set with a specific time delay (T_i^{EV}) and a percentage of represented EVs (n_i^{EV}) in per unit value. The two discrete distributions limit T_i^{EV} in the range of 0 s–4 s, with the centre of the probability at $\overline{T}^{\text{EV}}$.

The total EV fleet response is the summation of the nine first-order transfer functions representing each set i, as reported in (4).

$$H(s) = \sum_{i=1}^{9} H_i(s) = N^{\text{EV}} \sum_{i=1}^{9} \frac{n_i^{\text{EV}} e^{-T_i^{\text{EV}} s}}{1 + T_i^{\text{b}} s} \tag{4}$$

In the following, the simplified EV response includes linear modulation of EV charging current and synchronized EV activation time, whereas the realistic EV response accounts for discrete modulation of EV charging current and non-synchronized EV activation time.

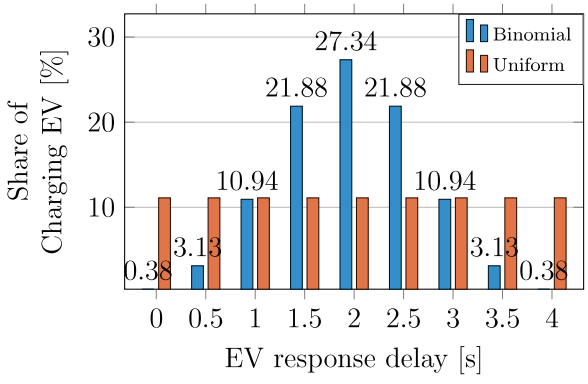

Fig. 2. Discrete probability distributions. For the uniform distribution, the share of EV charging is 11.11 %.

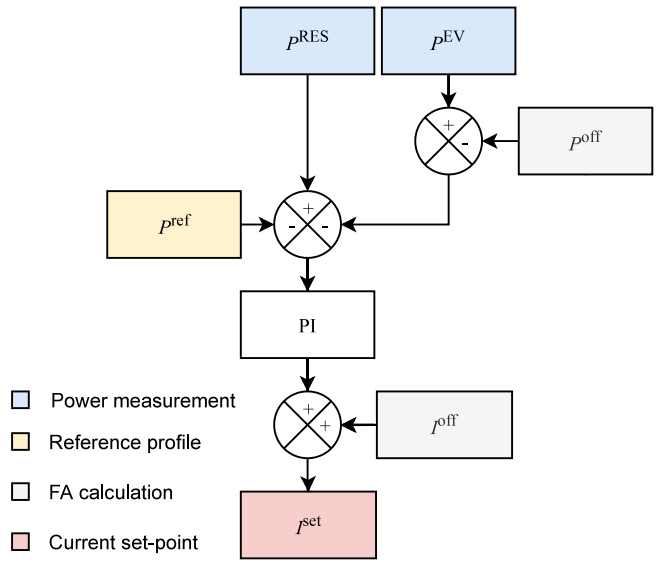

Fig. 3. Power controller scheme.

2.2. Power controller – PC

This section describes the PC, the smart charger based on EV fleet power consumption management. Fig. 3 shows the structure of the controller.

The considered PC is realized with a Proportional–Integral (PI) regulator with a back calculation anti-windup control [2]. The PC sets the current set-point I^{set} of each EV, based on the RES power production deviation (P^{RES}) from a desired reference power (P^{ref}). To quantify the EV fleet support, the EV fleet offset charging power (P^{off}) is calculated by the FA. knowing I^{off}, the voltage level (V) at which EVs are grid-connected, and N^{EV} (5). The charging power (P^{EV}), i.e. total power absorbed by the entire EV fleet, is subtracted by (P^{off}) to detect the deviation of charging power (ΔP^{EV}) from charging at I^{off}. Then, the power error signal (P^{ε}) sent to the regulator is derived as in (7).

$$P_t^{off} = \sqrt{3} \cdot V_t \cdot I^{off} \cdot N^{EV} \tag{5}$$

$$\Delta P_t^{EV} = P_t^{EV} - P_t^{off} \tag{6}$$

$$P_t^{\varepsilon} = P_t^{RES} - \Delta P_t^{EV} - P_t^{ref} \tag{7}$$

The PI regulator output is the deviation in EV current set-point (ΔI^{set}), obtained as the sum of a proportional term and an integral term. The first term is proportional to P^{ε}, while the second integrates past values of P^{ε} over time. The proportional gain K_P and the integral gain K_I of the regulator are tuned following the Ziegler–Nichols methodology and they are fixed for this study at 1.2 and 0.5, respectively. Then, the FA sums ΔI^{set} obtained from (8) to I^{off} to obtain I^{set}, and sets this charging set-point to all EVs in the fleet (9).

$$\Delta I_t^{set} = K_P \cdot P_t^{\varepsilon} + K_I \int_T P_t^{\varepsilon} dt \tag{8}$$

$$I_t^{set} = I^{off} + \Delta I_t^{set} \tag{9}$$

2.3. Energy controller – EC

This section describes the EC, the smart charger based on EV fleet energy consumption management. Fig. 4 shows the structure of the controller.

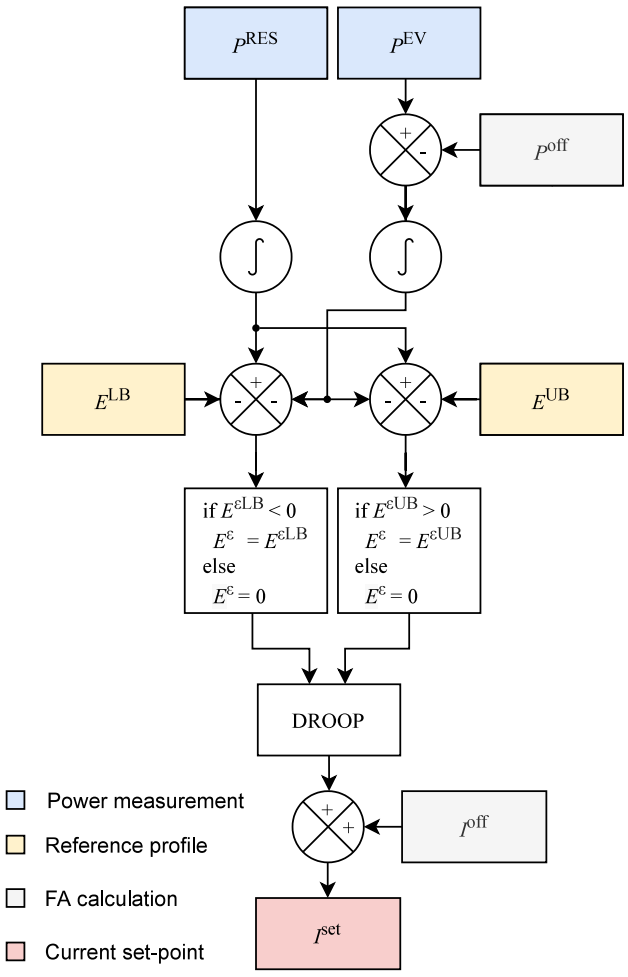

Fig. 4. Energy controller scheme.

The considered EC was derived for systems including stationary BESS and RES [1,2,18], and this is its first application to EV fleets. Therefore, the EC sets the I^{set} to each EV based on RES energy production deviations from the forecasted energy plan. On the one hand, the RES power production (P^{RES}) is integrated to obtain the associated energy production (E^{RES}) (10). On the other hand, P^{EV} is subtracted by P^{off} (5), and then integrated. This is done to detect the deviation in EV fleet charging energy (ΔE^{EV}) with respect to remaining at I^{off} (11).

$$E_t^{RES} = \int_T P_t^{RES} dt \tag{10}$$

$$\Delta E_t^{EV} = \int_T (P_t^{EV} - P_t^{off}) dt \tag{11}$$

Consequently, the EC control logic in Fig. 5 comes into play. The upper and lower energy bands, $\overline{UB}$ (i.e. line segment going from point U to B) and $\overline{LB}$, respectively, are introduced to ensure the EV fleet is able to compensate for the error in the forecasted energy plan. As long as E^{RES} evolves within the two bands, no control actions are taken because the production appears to follow what the VPP operator forecasted. If E^{RES} goes above/below the upper/lower energy band, the FA adjust the EV consumption accordingly.

The EC calculates the energy errors in respect to $\overline{UB}$ ($E^{\varepsilon UB}$) and $\overline{LB}$ ($E^{\varepsilon LB}$) as in (12) and (13), where E^{UB} and E^{LB} refer to the instantaneous energy value of $\overline{UB}$ and $\overline{LB}$, respectively. The

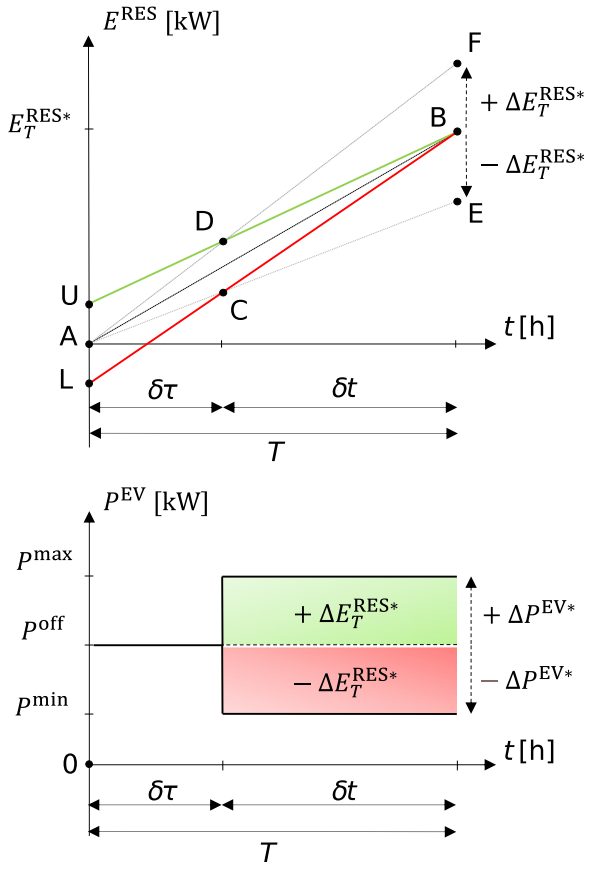

Fig. 5. Control logic for defining the starting point of upper and lower energy bands.

energy error signal (E^{ε}) sent to the regulator is defined in (14) and reported in Fig. 4. The larger the distance above $\overline{UB}$, the greater the positive E^{ε} sent, and vice versa, while E^{ε} is zero when in between the two bands.

$$E_t^{\varepsilon UB} = E_t^{RES} - \Delta E_t^{EV} - E_t^{UB} \tag{12}$$

$$E_t^{\varepsilon LB} = E_t^{RES} - \Delta E_t^{EV} - E_t^{LB} \tag{13}$$

$$E^{\varepsilon} = \begin{cases} E^{\varepsilon UB} & \text{if } E^{\varepsilon UB} > 0 \\ E^{\varepsilon LB} & \text{if } E^{\varepsilon LB} < 0 \\ 0 \end{cases} \tag{14}$$

To linearly relate E^{ε} to ΔI^{set}, the droop regulator equation defined in (15) is implemented. Since it is a proportional regulator, a positive E^{ε} gives a positive ΔI^{set}, thus I^{set} increases above I^{off} and ΔE^{EV} increases too. Vice versa, when a negative E^{ε} is detected, ΔI^{set} is negative, and ΔE^{EV} decreases. The nominal current I^{nom} and nominal energy E^{nom} are introduced to normalize input and output of the regulator, so that the droop constant (K_D) represents a pure droop. I^{nom} is defined as the amount of flexibility each EV can provide, calculated from the admitted charging range of the selected charger type as in (16), whereas E^{nom} is the nominal hourly energy production for the considered RES. K_D is fixed at 0.17%, and it is defined so as to 1 kWh deviation above/below the upper/lower energy bands corresponds to 1 A deviation in I^{set}. Lower K_D means higher regulator sensitivity to input signal variation.

$$\frac{E^{\varepsilon}}{E^{nom}} = K_D \cdot \frac{\Delta I^{set}}{I^{nom}} \tag{15}$$

$$I^{nom} = I^{max} - I^{min} \tag{16}$$

The EC was equipped with a fixed stiffness control logic in previous articles [1,2,18], meaning that points U and L in Fig. 5 had a manually predefined position along the ordinates. The authors propose a variable stiffness control logic, where points U and L move along the ordinates as function of:

- a control window (T) to define the following energy and power parameters.
- a forecasted RES energy production ($E_T^{RES^*}$) for each T.
- a maximum admitted RES energy production error ($\Delta E_T^{RES^*}$) in respect to $E_T^{RES^*}$ to be erased with the controller.
- the symmetrical admitted power deviation (ΔP^{EV^*}) above and below P^{off}. This deviation is function of I^{max} and I^{min}, which determine P^{max} and P^{min}.

Segments $\overline{AF}$ and $\overline{AE}$ represent the linear increase in E^{RES} if the energy production in T were distant $\Delta E_T^{RES^*}$ from $E_T^{RES^*}$, for over- and underproduction. Consequently, δt is defined as minimum required time to absorb $\pm\Delta E_T^{RES^*}$ with the available ΔP^{EV^*} (17), while $\delta\tau$ is the complementary time in T, meaning the maximum waiting time to later absorb $\Delta E_T^{RES^*}$ (18).

$$\delta t = \frac{\Delta E_T^{RES^*}}{\Delta P^{EV^*}} \tag{17}$$

$$\delta\tau = T - \delta t \tag{18}$$

Consequently, the known points in the EC control logic are:

$$B : (x^B, y^B) = (T, E_T^{RES^*}) \tag{19}$$

$$C : (x^C, y^C) = \left(\delta\tau, \frac{E_T^{RES^*} - \Delta E_T^{RES^*}}{T} \cdot \delta\tau\right) \tag{20}$$

$$D : (x^D, y^D) = \left(\delta\tau, \frac{E_T^{RES^*} + \Delta E_T^{RES^*}}{T} \cdot \delta\tau\right) \tag{21}$$

$$E : (x^E, y^E) = (T, E_T^{RES^*} - \Delta E_T^{RES^*}) \tag{22}$$

$$F : (x^F, y^F) = (T, E_T^{RES^*} + \Delta E_T^{RES^*}) \tag{23}$$

Finally, $\overline{UB}$ and $\overline{LB}$ energy bands are obtained solving (24) and (25), detecting the variable position of points U and L, respectively.

$$U : \frac{y - y^D}{y^B - y^D} = \frac{x - x^D}{x^B - x^D} \tag{24}$$

$$L : \frac{y - y^C}{y^B - y^C} = \frac{x - x^C}{x^B - x^C} \tag{25}$$

Greater $\Delta E_T^{RES^*}$ or smaller ΔP^{EV^*} give closer control bands, meaning points U and L get closer to A, and vice versa. The closer the control bands, the stiffer the control, collapsing in a single-band control logic in case the two bands are overlapped on $\overline{AB}$.

3. Test case

The influence of simplified and realistic EV response in power and energy controllers is investigated in a VPP located at the Danish town of Aakirkeby, Bornholm [19]. The VPP is composed of the Kalby WF and a potential aggregation of EVs, interlinked through the VPP operator and the FA. Thus, this section describes each entity and their communication infrastructure with the help of the system overview represented in Fig. 6.

3.1. Kalby wind farm and VPP operator

Kalby WF has a nominal power of 6 MW, and it is connected to the 10 kV bus of Aakirkeby substation. As a consequence, the required E^{nom} is fixed at 6 MWh for the energy controller

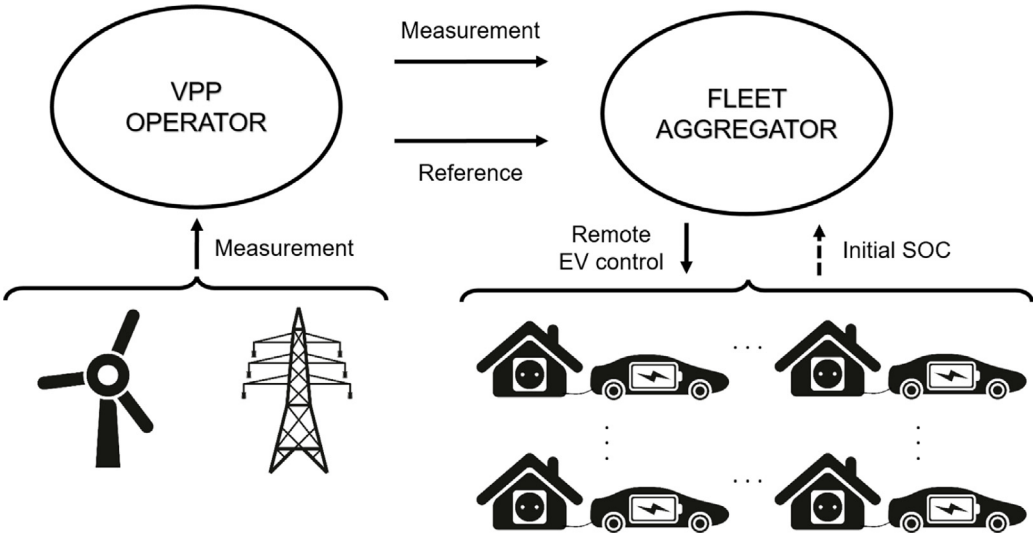

Fig. 6. System overview of the test case.

described in Section 2.3. The role of the VPP operator is to both collect measurements from the WF and create the reference signal, which will be used as input to the controllers.

Data of the active power injected in a 10-s resolution at the 10 kV bus by the Kalby WF over a 12 h timeline (21st January 2020 at 6pm–22nd January 2020 at 6am) are used in the analysis. To observe the impact of the WF power fluctuations on the system, fluctuations are quantified with the CV, defined as the ratio between standard deviation and mean power production of the WF (26).

$$CV = \frac{STD(P^{\mathrm{RES}})}{mean(P^{\mathrm{RES}})} \tag{26}$$

3.2. EV fleet and fleet aggregator

A potential scenario with 100% EV penetration in Aakirkeby is investigated by modelling the EV fleet as an aggregation feeder connected at the 10 kV bus of Aakirkeby substation.

An EV population of 40 kWh Lithium-ion battery and average energy consumption of 0.2 kWh/km is considered, including 90% charging efficiency [20], and it is assumed that EVs can be charged once per day [21]. Since the choice of representing only a EV typology in the fleet, the time constant T^{b} in Section 2.1 is equal to 0.2 s [17]. According to the IEC 61851 standard, the three-phase unidirectional domestic charger (CH3PH) (rated power 11 kW, 400 V, $I^{\max}$ 16 A, $I^{\min}$ 6 A) is chosen. This charging power is common in Danish households with the common three-phase residential grid connection. As a consequence, I^{off} is set at 11 A in the EV fleet described in Section 2.1, and the required I^{nom} in Section 2.3 at 10 A. For the sake of simplicity, each CH3PH is considered to be directly connected to the 10 kV bus, thus neglecting transformer and low-voltage distribution losses.

The single user charging behaviour plays a key role, defining when, how many, and with which SOC the EVs are plugged-in and available to provide flexibility to the VPP. According to the Danish National Travel Survey [22], the average distance driven is 34 km/day on the island of Bornholm, cars are used mainly between 6am–6pm, and one of every two citizens owns a car. For the considered EV penetration scenario, and taking into account that there were 2108 inhabitants in the town on January 2020, it is assumed that 1067 EVs are available in the fleet. However, no real EV data are available for the investigated area. Thus, pseudo-real (simulated) driving and charging profiles of an EV fleet are derived from data on the real EV driving and charging behaviour by the Danish population [23]. From the reported weekly analysis, the average amount of charged EVs at home is 45% of the population, with an average plug-in SOC equal to 62%. Since the considered total number of EVs is 1067, the corresponding number of daily charged EVs in the EV fleet model is 480.

The FA role is to optimally manage the EV fleet composed of 480 EVs, to guarantee the driving needs and maximize the VPP ancillary services provision. A centralized control strategy is considered for this analysis [24]. This strategy allows the FA to schedule the charging time for each EV and to directly control I^{set}, applying the same control signal to all the considered EVs in the aggregation. From the EV fleet perspective, EV owners allow the FA to fully control their vehicles when grid-connected. Consequently, the FA divides the EV fleet into six groups (G1–G6), each counting for 80 EVs (which corresponds to N^{EV} in the EV fleet model), and charged for two hours consecutively via CH3PH between 6pm and 6am. Considering the plug-in SOC of 62% and I^{off} of 11 A, each group would reach a maximum SOC equal to 96.3% (ΔSOC of +34.3% from plug-in SOC), covering the average daily energy travel consumption (34 km/day amounts to 17% of the SOC for the chosen EV battery size).

The taken choices from the FA open for multiple benefits. First, due to the defined I^{off}, EVs can increase or decrease their energy consumption if required from the controllers, enhancing their flexibility as long as possible in the charging time. Concurrently, splitting the EV fleet into groups and spreading their charging time between the 12 h timeline prevents simultaneous charging of all EVs. This results in decreasing grid impact and longer time periods within which EVs are available to provide ancillary services to the VPP.

3.3. Communication infrastructure

A minimal communication infrastructure is required to share signals among the entities. The VPP operator sends both measurement and reference signal to the FA. The FA, in turn, controls I^{set} comparing the measurement signal with the reference signal to be satisfied, and calculates power or energy errors depending on the considered controller.

According to the IEC 61851, the CH3PH does not have two-way communication capability, thus signals can be sent from the FA to each EV, but not vice versa. Therefore, to detect if the EVs effectively follow the I^{set}, P^{EV} is measured directly at the point of

the substation, where the EV fleet is connected. Moreover, a real time monitoring of the SOC evolution for each EV charging is not possible with the CH3PH. Thus, it is assumed that when EVs are plugged-in, only the initial SOC is communicated from each EV back to the FA.

4. Analysed scenarios and results

This section presents results from the following scenarios:

A. Benchmark scenario: the WF power production without the EV support is used for defining reference power profile for the PC and hourly VPP energy targets for the EC.
B. EV penetration scenario: the EV fleet contributes actively as WF support, applying the following controllers (one at a time):

- PC.
- EC with variable stiffness control logic.
- EC with single-band control logic.

For each controller, the simplified and realistic EV response are applied to detect their influence on the VPP output. All analysis were run with the software DIgSILENT PowerFactory®.

4.1. Benchmark scenario

Fig. 7a illustrates the historical WF power production in the considered 12 h timeline. Due to sudden and uncontrollable wind speed variations, the instantaneous WF power production is highly fluctuating, and the CV counts for 11.68. Table 1 collects the hourly WF energy production.

The hourly VPP energy forecast is manually chosen to determine a ±5% error in the hourly WF energy production, with respect to the forecast [25]. The mean absolute error (MAE), both in absolute and relative terms, is calculated over the 12 h timeline. Notably, the scheduling is defined to represent an underproduction in between 6pm–8pm, 10pm–11pm, 12am–2am, 4am–5am, while an overproduction during the remaining hours. For the PC, the reference power profile is a set of constant hourly power values, where each of them corresponds to the hourly VPP energy forecast, aiming at increasing/decreasing the mean injected WF power production (Fig. 7b). For the EC, each energy target $E_T^{RES^*}$ in T, where T equals to one hour, corresponds to a hourly VPP energy forecast.

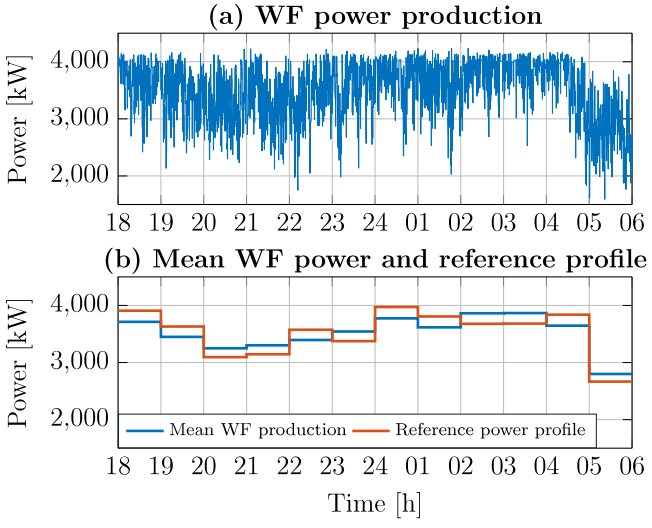

Fig. 7. (a) WF power production in the 12 h timeline and (b) mean WF production with the defined reference power profile.

Table 1
Hourly VPP forecast and WF production with related energy errors.

Time [h]	Forecast [kWh]	Production [kWh]	Error [kWh]	[%]
18–19	3908	3713	−195	−5
19–20	3631	3449	−182	−5
20–21	3095	3250	155	5
21–22	3145	3302	157	5
22–23	3574	3395	−179	−5
23–24	3375	3544	169	5
24–01	3972	3774	−198	−5
01–02	3807	3617	−190	−5
02–03	3679	3863	184	5
03–04	3682	3866	184	5
04–05	3828	3646	−182	−5
05–06	2666	2800	134	5
MAE	–	–	176	5

4.2. EVs penetration scenario

The following analysis considers the EV fleet available for acting as WF support between 6pm and 6am. Thus, it highlights the influence of the realistic EV response on the overall VPP output, and compares the two proposed EV smart charging controllers from both WF and EV fleet perspectives.

4.2.1. Impact of simplified and realistic EV response on the VPP output

The contribution of the PC is shown in Fig. 8, for a random time window of 60 s. It shows the resulting VPP power production (Fig. 8a and b) and the average EV fleet charging current (Fig. 8c and d), following linear (Fig. 8a and c) and 1A-discrete (Fig. 8b and d) charging modulation, and highlighting synchronized/non-synchronized EV activation time. The VPP power production with PC clearly shows the influence due to simplified and realistic EV response. Indeed, the VPP power production oscillates around the reference power set-point when a 1A-discrete modulation is applied, being unable to stabilize (Fig. 8b and d between 19:15:30 and 19:15:45). Finally, when min/max EV charging current is requested, the EV fleet cannot adequately modulate the VPP power production, thus the reference power set-point cannot be achieved (Fig. 8a and b at 19:15:15 and 19:16:00).

The contribution of the EC with variable stiffness (Fig. 9a, c and e) and single-band (Fig. 9b, d and f) control logic are shown for the same time window of 60 s. For both control logic, the resulting VPP energy production (Fig. 9a and b), following linear (Fig. 9c and d) and 1A-discrete (Fig. 9e and f) charging modulation is reported. The EV charging current is visibly influenced by the required linear or 1A-discrete modulation. Specifically, the synchronized/non-synchronized EV activation time can be detect mainly when 1A-discrete modulation is imposed. However, the resulting VPP energy production follows the EC requests without showing any substantial difference between simplified and realistic EV response (Fig. 9a for the variable stiffness control logic, Fig. 9b for the single-band control logic).

4.2.2. Hourly energy management

This section compares how the presented controllers help the WF to achieve the hourly VPP energy plan by minimizing energy errors, both when a simplified and a realistic EV response is applied. The hourly energy targets and the reference power profile are defined from the hourly VPP energy forecast. Thus, Table 2 gathers the resulting VPP energy output influenced by the EV fleet.

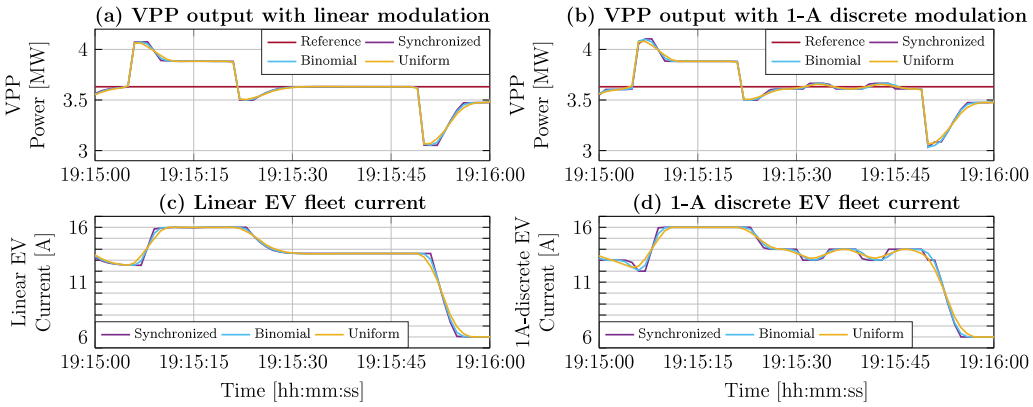

Fig. 8. Performance of the PC with (a)–(c) linear modulation and (b)–(d) 1A-discrete modulation: (a)–(b) reference power signal and VPP power production, (c)–(d) average EV fleet charging current.

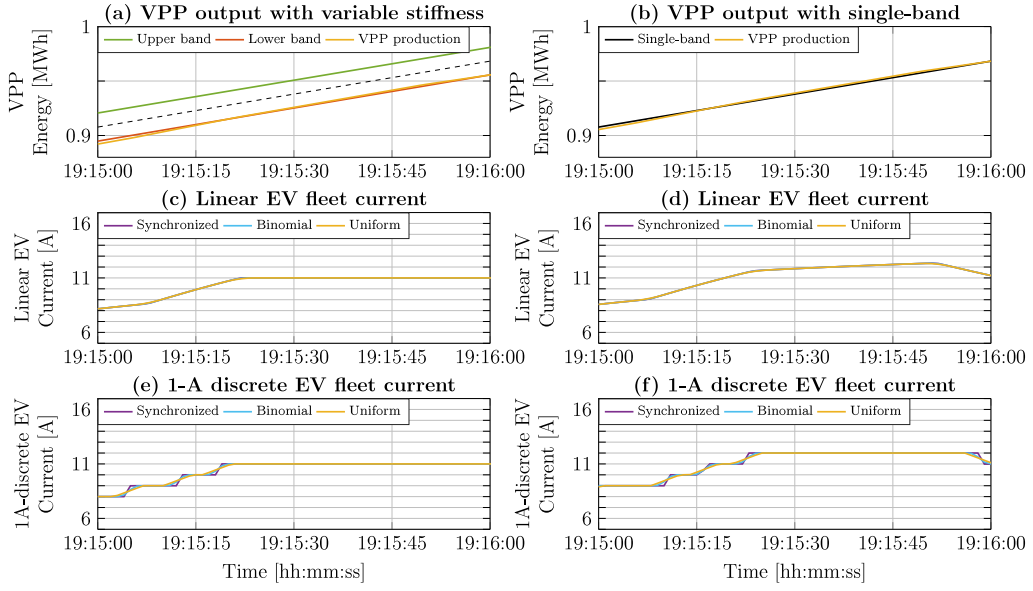

Fig. 9. Performance of the EC with (a)–(c)-(e) variable stiffness control logic and (b)–(d)-(e) single-band control logic: (a)–(b) energy bands and VPP energy production, average EV fleet charging current caused by (c)–(d) linear modulation and (e)–(f) 1A-discrete modulation.

Overall, the results are not influenced by charging modulation and EV activation time. The time period T being one hour for this test case, the realistic EV response does not produce any difference in respect of considering the simplified EV response. Thus, the latter can be modelled and considered for similar application without committing noticeable errors. Moreover, it is seen that the EC achieves a smaller hourly VPP energy error than the PC. In particular, the single-band control logic results in better energy management than with a variable stiffness control logic. Indeed, the MAE of 5% (without EV support) drops to 2.66% with the PC, 0.73% with the variable stiffness EC, and 0.65% with the single-band EC. Thus, if the energy management is the primary objective, the EV smart charging controllers with energy bands are suggested, since they show a 75% smaller MAE in respect to the PC.

4.2.3. Wind power fluctuations

It is investigated how both controller decrease the injection of wind power fluctuations into the grid. For each controller, the CV is calculated for both the simplified and the realistic EV response. Table 3 collects the results.

Overall, charging modulation affects the resulting VPP power fluctuations more than the EV activation time, mainly with the PC. Indeed, a linear modulation of the charging current allows for following the reference power profile more precisely compared to the 1A-discrete modulation, resulting in a lower CV. Considering the EV activation time, if the EV response were represented with a uniform distribution the VPP power fluctuations would be lower than with a binomial or synchronized EV response. Consequently, if a non-synchronized EV activation time must be chosen to estimate the CV and err in the side of safety, the binomial is preferred to the uniform distribution. However, the analysis shows that the synchronized EV activation time can be considered for similar applications without committing noticeable errors. Averaging the obtained results, the PC brings a decrease of 28% to the CV in respect to the benchmark scenario, followed by the EC with single-band control logic (−7%), lastly with variable stiffness control logic (−4%). Thus, if the power smoothing is the main objective, a linear modulation of the EV charging current with the PC is suggested. This in fact shows from four to six times greater CV reduction than with single-band and variable stiffness EC, respectively.

4.2.4. Flexibility of EV charging

Fig. 10 shows the average EV charging current profiles with the three controllers: Fig. 10a the PC, Fig. 10b the EC with variable stiffness and Fig. 10c the EC with single-band control logic.

Table 2
Hourly VPP production and resulting errors in respect to the VPP forecast.

Time	PC			EC					
[h]				Variable stiffness			Single-band		
	Production [kWh]	Error [kWh]	[%]	Production [kWh]	Error [kWh]	[%]	Production [kWh]	Error [kWh]	[%]
18–19	3804	−104	−2.66	3908	0.00	0.00	3909	1.00	0.00
19–20	3515	−116	−3.19	3611	−20.0	−0.55	3618	−13.0	−0.36
20–21	3190	95.0	3.07	3124	29.0	0.94	3125	30.0	0.97
21–22	3226	81.0	2.58	3182	37.0	1.18	3179	34.0	1.08
22–23	3449	−125	−3.50	3574	0.00	0.00	3574	0.00	0.00
23–24	3442	67.0	1.99	3383	8.00	0.24	3379	4.00	0.12
24–01	3873	−99.0	−2.49	3954	−18.0	−0.45	3959	−13.0	−0.33
01–02	3689	−121	−3.10	3790	−17.0	−0.45	3796	−11.0	−0.29
02–03	3710	31.0	0.84	3688	9.00	0.24	3686	7.00	0.19
03–04	3747	65.0	1.77	3749	67.0	1.82	3747	65.0	1.77
04–05	3677	−151	−3.94	3719	−109	−2.85	3724	−104	−2.72
05–06	2739	73.0	2.74	2666	0.00	0.00	2666	0.00	0.00
MAE	–	94.0	2.66	–	26.2	0.73	–	23.5	0.65

Table 3
CV analysis and its reduction δCV in respect to benchmark with PC and EC.

Charging current modulation	EV response	PC		EC			
				Variable stiffness		Single-band	
		CV [/]	δCV [%]	CV [/]	δCV [%]	CV [/]	δCV [%]
Linear	Synchronized	8.27	29.2	11.19	4.2	10.84	7.2
	Binomial	8.20	29.8	11.19	4.2	10.85	7.1
	Uniform	8.15	30.2	11.18	4.3	10.84	7.2
1A-discrete	Synchronized	8.72	25.3	11.21	4.0	10.88	6.8
	Binomial	8.61	26.3	11.21	4.0	10.89	6.8
	Uniform	8.52	27.1	11.20	4.1	10.87	6.9

The figure demonstrates that the stiffer the controller, the more frequent the variations in the EV fleet charging current. Indeed, the second-by-second adjustment required by the PC is well visible, whereas both ECs are less strict. The EC with single-band control logic results in having more visible variations in respect to the variable stiffness EC. The PC reduces VPP power fluctuations, as shown in Table 2, while taking advantage of the intrinsic flexibility of charging EVs. Furthermore, EVs stop charging when 100% SOC is reached (e.g at 10pm and at 4am) and the support to VPP is suspended (further described in Section 4.2.5).

4.2.5. SOC analysis

As described in Section 3.2, the FA divides the EV fleet into six groups of 80 EVs each. The FA cannot use the SOC as decision variable to modulate the EVs charging set-point since the SOC tracking is not available with the considered CH3PH chargers. Thus, only the plug-in SOC of 62 % is known, whereas the achieved SOC after providing VPP support for two hours consecutively is not detectable. However, for the sake of validating the influence that PC and EC has on the EVs charging for two hours consecutively, the FA estimates the final SOC by knowing the initial SOC and the charged energy. The SOC analysis is processed along with the hourly VPP energy forecast. Indeed, the WF under- and overproduction affects the EV fleet charging current and the overall SOC. Table 4 collects the final SOC for each charging group (G1–G6).

On the one hand, groups G2 and G5 achieve the full charge because the WF energy production is underestimated by the VPP operator for two consecutive hours. On the other hand, groups G1 and G4 show a SOC 5%–10% lower than the predicted final SOC of 96.3% because the WF energy production is overestimated by the VPP operator for two consecutive hours. Although EVs are not fully charged, a minimum ΔSOC of +24% is ensured, clearly satisfying the 17% EV owners' driving needs for the upcoming day.

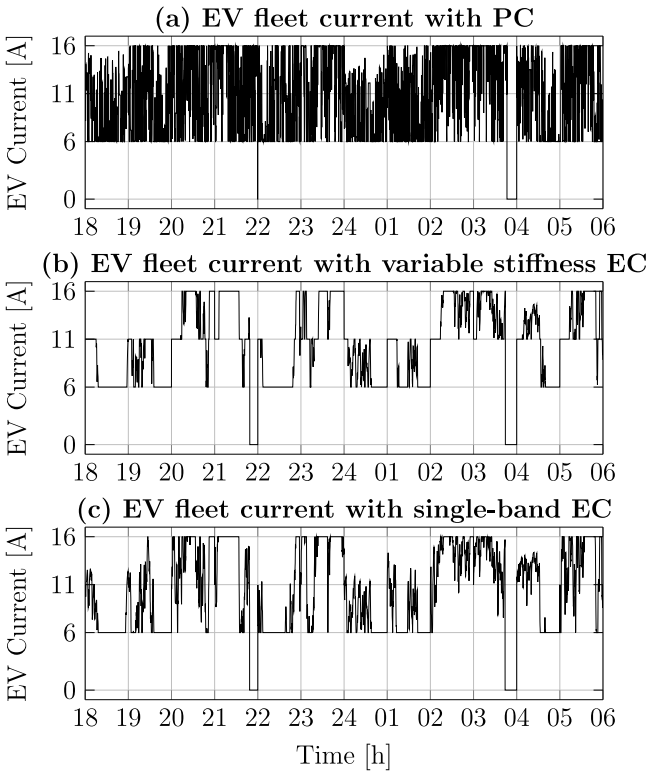

Fig. 10. Average EV fleet charging current with (a) PC, (b) EC with variable stiffness control logic, (c) EC with single-band control logic.

Table 4
SOC analysis and its increase ΔSOC in respect to the plug-in SOC of 62%.

Charging group and time [h]	PC		EC			
			Variable stiffness		Single-band	
	SOC [%]	ΔSOC [%]	SOC [%]	ΔSOC [%]	SOC [%]	ΔSOC [%]
(G1) 18–20	91.9	29.9	86.3	24.3	86.0	24.0
(G2) 20–22	100	38.0	100	38.0	100	38.0
(G3) 22–24	97.6	35.6	95.8	33.8	95.9	33.9
(G4) 24–02	91.5	29.5	86.3	24.3	86.0	24.0
(G5) 02–04	100	38.0	100	38.0	100	38.0
(G6) 04–06	96.7	34.7	98.1	36.1	97.9	35.9

Additionally, both PC and EC allow to decrease the average final SOC among the considered groups. Only part of the EV fleet is charged at 100% at the end of the charging session (groups G2 and G5). The lower average EV fleet SOC helps with lowering the deterioration of the battery, while providing support to the WF production. The SOC analysis does not show any difference between simplified and realistic EV response.

5. Conclusion

In this paper, a simplified and a realistic response of an EV fleet were modelled and compared. The realistic EV response accounts for non-synchronized activation time and discrete EV charging current modulation, while the simplified EV response considers synchronized activation time and linear EV charging current modulation. The analysis was realized by comparing the two EV responses in a PC and an EC when controlling the unidirectional EV fleet charging to support the fluctuating output of a WF.

The proposed modelling and control approaches were applied to historical 10-s generation data of a 6 MW WF, part of a VPP on the Danish island of Bornholm. To represent the potential aggregation of EVs with the uncertainty related to their charging availability, real Danish driving data were considered.

The analysis shows that the charging modulation type had a major impact to the VPP output in respect to the selected EV activation time for representing the EV fleet response. Indeed, a combination of the PC and the 1A-discrete modulation of the EV charging current could cause oscillations in the VPP power output, which were not observed in cases when either the linear modulation or the EC are considered. The non-synchronized EV activation time had, however, a negligible impact on the outcomes in respect to a synchronized EV activation time. Thus, the synchronized EV activation time can be considered for future investigations with similar time delays, without committing noticeable errors.

From the comparison between PC and EC, the results show that the EC allowed reducing the imbalance between the actual and forecasted energy production by 87%, whereas the PC – only by 47%. On the contrary, the usage of the PC led to decreasing wind power fluctuations by 28%, whereas the EC – only by 7%. Moreover, the proposed variable stiffness control logic for the EC brought comparable improvements as with the single-band control band logic. However, the single-band control logic required a more frequent variation of the EV charging current when providing support. Finally, the VPP energy production when controlling the EV fleet with a constant hourly reference power via PC is not the equivalent to when the EC with a linear hourly energy evolution is considered, despite the equality of the approaches from a mathematical perspective.

In terms of power system loading, the suggested choice of distributing EVs through the night decreased the simultaneous charging power from a large EV fleet. From the EV owners' perspective, the vehicles were charged for two consecutive hours. The achieved final SOC satisfies future driving needs, while lowering degradation of batteries.

The EV fleet, the PC and the EC can be applied to other configurations of VPP, integrating EVs with other fluctuating RES. However, an EV fleet of different size or geographical localization may require partial changes in the EV fleet characterization and modelling.

The proposed VPP will be further investigated in future research. First, the EV smart charging controllers will benefit from knowing the evolution of the SOC, directly conditioning the FA decision making. Second, the realistic EV response will be applied to other short term ancillary services (e.g. frequency regulation) to better estimate the influence when supporting grid stability. Finally, the EV fleet model will be further improved considering aspects of battery degradation when providing services in future VPP integration.

CRediT authorship contribution statement

Mirko Ledro: Conceptualization, Methodology, Writing – original draft, Writing – review & editing, Formal analysis, Investigation. **Lisa Calearo:** Conceptualization, Methodology, Writing – review & editing. **Jan Martin Zepter:** Conceptualization, Methodology, Writing – review & editing. **Tatiana Gabderakhmanova:** Conceptualization, Methodology, Writing – review & editing. **Mattia Marinelli:** Conceptualization, Methodology, Writing – review & editing, Supervision, Funding acquisition, Project administration.

Declaration of competing interest

The authors declare that they have no known competing financial interests or personal relationships that could have appeared to influence the work reported in this paper.

Funding

This work has received funding from the H2020 INSULAE, Denmark project under the Grant Agreement No. 824433. For more information, visit http://insulae-h2020.eu/.

References

[1] M. Marinelli, F. Sossan, G.T. Costanzo, H.W. Bindner, Testing of a predictive control strategy for balancing renewable sources in a microgrid, IEEE Trans. Sustain. Energy 5 (4) (2014) 1426–1433, http://dx.doi.org/10.1109/TSTE.2013.2294194.

[2] F. Baccino, M. Marinelli, F. Silvestro, O. Camacho, F. Isleifsson, P. Norgard, Experimental validation of control strategies for a microgrid test facility including a storage system and renewable generation sets, 2012, http://dx.doi.org/10.1049/cp.2012.0830.

[3] D.I. Stroe, A. Zaharof, F. Iov, Power and energy management with battery storage for a hybrid residential PV-wind system – A case study for Denmark, Energy Procedia 155 (2018) 464–477, http://dx.doi.org/10.1016/J.EGYPRO.2018.11.033.

[4] S. Gao, K.T. Chau, C. Liu, D. Wu, C.C. Chan, Integrated energy management of plug-in electric vehicles in power grid with renewables, IEEE Trans. Veh. Technol. 63 (7) (2014) 3019–3027, http://dx.doi.org/10.1109/TVT.2014.2316153.

[5] K. Kouka, A. Masmoudi, A. Abdelkafi, L. Krichen, Dynamic energy management of an electric vehicle charging station using photovoltaic power, Sustain. Energy Grids Netw. 24 (2020) 100402, http://dx.doi.org/10.1016/J.SEGAN.2020.100402.

[6] W. Wang, P. Chen, D. Zeng, J. Liu, Electric vehicle fleet integration in a virtual power plant with large-scale wind power, IEEE Trans. Ind. Appl. 56 (5) (2020) 5924–5931, http://dx.doi.org/10.1109/TIA.2020.2993529.

[7] M. Raoofat, M. Saad, S. Lefebvre, D. Asber, H. Mehrjedri, L. Lenoir, Wind power smoothing using demand response of electric vehicles, Int. J. Electr. Power Energy Syst. 99 (2018) 164–174, http://dx.doi.org/10.1016/j.ijepes.2017.12.017.

[8] G. Haddadian, N. Khalili, M. Khodayar, M. Shahidehpour, Optimal coordination of variable renewable resources and electric vehicles as distributed storage for energy sustainability, Sustain. Energy Grids Netw. 6 (2016) 14–24, http://dx.doi.org/10.1016/J.SEGAN.2015.12.001.

[9] M. Honarmand, A. Zakariazadeh, S. Jadid, Integrated scheduling of renewable generation and electric vehicles parking lot in a smart microgrid, Energy Convers. Manage. 86 (2014) 745–755, http://dx.doi.org/10.1016/j.enconman.2014.06.044.

[10] A. Tavakoli, M. Negnevitsky, D.T. Nguyen, K.M. Muttaqi, Energy exchange between electric vehicle load and wind generating utilities, IEEE Trans. Power Syst. 31 (2) (2016) 1248–1258, http://dx.doi.org/10.1109/TPWRS.2015.2418335.

[11] P. Kou, D. Liang, L. Gao, F. Gao, Stochastic coordination of plug-in electric vehicles and wind turbines in microgrid: A model predictive control approach, IEEE Trans. Smart Grid 7 (3) (2016) 1537–1551, http://dx.doi.org/10.1109/TSG.2015.2475316.

[12] V.T. Samundsson, M. Rezkalla, A. Zecchino, M. Marinelli, Aggregation of single-phase electric vehicles for frequency control provision based on unidirectional charging, in: 2017 52nd International Universities Power Engineering Conference, UPEC 2017, IEEE, 2017, pp. 1–6, http://dx.doi.org/10.1109/UPEC.2017.8231867.

[13] R.J. Askjær, P.B. Andersen, A. Thingvad, M. Marinelli, Demonstration of a technology neutral control architecture for providing frequency control using unidirectional charging of electric vehicles, in: Proceedings of the 55th International Universities Power Engineering Conference IEEE, 2020.

[14] S. Habib, M.M. Khan, F. Abbas, H. Tang, Assessment of electric vehicles concerning impacts, charging infrastructure with unidirectional and bidirectional chargers, and power flow comparisons, Int. J. Energy Res. 42 (11) (2018) 3416–3441, http://dx.doi.org/10.1002/er.4033.

[15] L. Calearo, A. Thingvad, M. Marinelli, Modeling of battery electric vehicles for degradation studies, in: 2019 54th International Universities Power Engineering Conference, UPEC 2019 - Proceedings, 8893474, IEEE, 2019, 8893474, http://dx.doi.org/10.1109/UPEC.2019.8893474.

[16] International Electrotechnical Commission, IEC 61851 - Electric vehicle conductive charging system – Electric vehicles requirements for conductive connection of an a.c./d.c. power supply | IEC Webstore.

[17] A. Zecchino, Electric Vehicles in the Nordic Countries: Control Strategies for Coordinated Grid Services (Ph.D. thesis), Technical University of Denmark, 2019.

[18] M. Marinelli, F. Sossan, F.R. Isleifsson, G.T. Costanzo, H. Bindner, Day-ahead scheduling of a photovoltaic plant by the energy management of a storage system, in: Proceedings of the Universities Power Engineering Conference, APA, 2013, http://dx.doi.org/10.1109/UPEC.2013.6715023.

[19] T. Gabderakhmanova, J. Engelhardt, J.M. Zepter, T.M. Sorensen, K. Boesgaard, H.H. Ipsen, M. Marinelli, Demonstrations of DC microgrid and virtual power plant technologies on the danish island of Bornholm, in: UPEC 2020 - 2020 55th International Universities Power Engineering Conference, Proceedings, IEEE, 2020, http://dx.doi.org/10.1109/UPEC49904.2020.9209853.

[20] A. Thingvad, P.B. Andersen, T. Unterluggauer, C. Treholt, M. Marinelli, Electrification of personal vehicle travels in cities - quantifying the public charging demand, ETransportation 9 (2021) 100125, http://dx.doi.org/10.1016/j.etran.2021.100125.

[21] L. Calearo, H. Ziras, K. Sevdari, M. Marinelli, Comparison of smart charging and battery energy storage system for a PV prosumer with an EV, in: Proceedings of ISGT Europe 2021, IEEE, http://dx.doi.org/10.1109/ISGTEurope52324.2021.9640120.

[22] The Danish National Travel Survey - Center for Transport Analytics.

[23] L. Calearo, A. Thingvad, K. Suzuki, M. Marinelli, Grid loading due to EV charging profiles based on pseudo-real driving pattern and user behavior, IEEE Trans. Transp. Electrif. 5 (3) (2019) 683–694, http://dx.doi.org/10.1109/TTE.2019.2921854.

[24] J. Hu, H. Morais, T. Sousa, M. Lind, Electric vehicle fleet management in smart grids: A review of services, optimization and control aspects, Renew. Sustain. Energy Rev. 56 (2016) 1207–1226, http://dx.doi.org/10.1016/j.rser.2015.12.014.

[25] J. Wu, B. Zhang, H. Li, Z. Li, Y. Chen, X. Miao, Statistical distribution for wind power forecast error and its application to determine optimal size of energy storage system, Int. J. Electr. Power Energy Syst. 55 (2014) 100–107, http://dx.doi.org/10.1016/j.ijepes.2013.09.003.